

Microwave Journal



Editor's Note: This article is based on US Patent Application No. 62/469,752, March 10, 2017. It describes a new micro-electromechanical-system (MEMS) switch technology in a three-part article over the next three issues. Part I reports on MEMS switch topologies including a new defective ground structure (DGS) and metamaterial inspired capacitive contact MEMS switch; Part II reports methods to reduce stiction effects in a resistive contact MEMS switch; and Part III discusses methods to reduce static friction (or stiction) effects in a capacitive contact MEMS switch for applications in modern electronic circuits and 5G communications.



A Microelectromechanical Switch with Metamaterial Contacts, Part I: Concepts and Technology

Shiban K. Koul and Chaitanya Mahajan
C.A.R.E, Indian Institute of Technology, Delhi, India

Ajay K. Poddar and Ulrich L. Rohde
Synergy Microwave, N.J., USA

A new MEMS switch with improved isolation, insertion loss and reduced liability for stiction is reported for the applications in high frequency electronics and communication systems. MEMS switches are suitable for signal routing for transmit and receive applications, switched line phase shifters for phased array antennas, wide band tuning networks and high precision instrumentation applications. Typical MEMS switches are categorized by the contact methods, capacitive (metal-insulator-metal) and resistive (metal-to-metal).

MEMS switches are typically a silicon-based integrated circuit technology with moving mechanical parts that are released by means of etching sacrificial silicon dioxide layers. MEMS switches include a signal line having an input port and output port between first and second ground planes, and a beam for controlling the activation. In this article, the variation of the switch architecture includes one or more DGS formed in the first and second ground planes, and a corresponding secondary deflectable beam positioned over each DGS. For reducing the vulnerability of

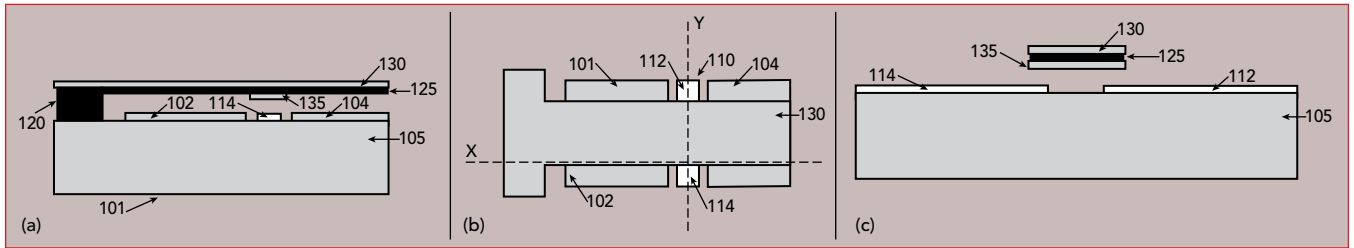
stiction, the switch incorporates an artificial engineering structure known as metamaterial for creating the repulsive Casimir interactions to mitigate the stiction related issues in switches.¹⁻⁶

Compared with PIN diodes or field effect transistor switches, MEMS switches offer lower cost and improved performance (power consumption, isolation, insertion loss and linearity). However, MEMS switches can encounter several drawbacks: high actuation voltages, high insertion loss and poor return loss. In addition to this, MEMS switches are susceptible to electromechanical failure after

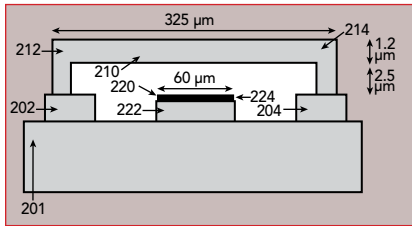
many switching cycles, especially under hot switching conditions. For instance, the switch may fail due to stiction buildup. When the movable part of the switch is pulled into contact with another component of the system (e.g., a signal line); the static friction can cause the switch to become stuck and non-functional. It may require a high voltage to overcome the stiction force. But at low voltage, the switch can remain "welded" to the component.

MEMS SWITCHES

MEMS switches are usually categorized by the contact methods: capacitive (metal-insulator-metal)

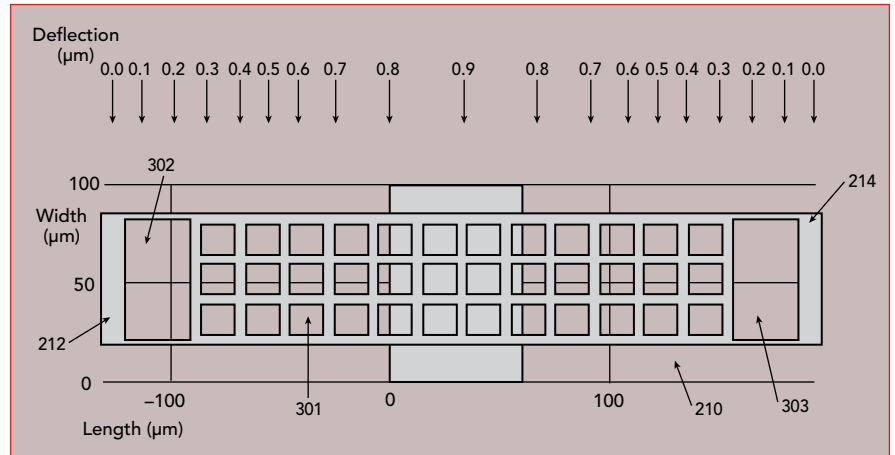


▲ Fig. 1 A typical MEMS switch: (a) cross-sectional view along X-axis, (b) top view and (c) cross-sectional view along Y-axis.



▲ Fig. 2 Shows Side-View of switch using a doubly supported cantilever beam designed above a coplanar waveguide. and resistive (metal-to-metal). Capacitive switches use a thin layer of dielectric material to separate two conducting electrodes when actuated. The dielectric layer prevents direct metal-to-metal contact. Therefore, stiction of contacts due to thermal energy is less of a concern. However, the thin layer of dielectric material will only conduct signals with reasonable insertion loss when the coupling between conductor electrodes is above a certain frequency. Moreover, the isolation bandwidth of capacitive switches is limited by the ratio between the ON and OFF capacitances. Metal-to-metal switches use physical contact of metal with low contact resistance to achieve low insertion loss when actuated. Therefore, the metal-to-metal MEMS switches can be operated from DC to RF frequency with isolation defined by the coupling capacitance of the electrodes when the switch is open. The metal-to-metal contact is made by surface asperities and the true contact area is much smaller than the apparent contact area. For the metal-to-metal contact to have low contact resistance, some plastic deformation of the asperities is required.

In general, as the pull-down force increases, the asperity deformation increases and the contact resistance decreases. However, adhesion of the contact point is proportional to the contact area and the temperature associated with the degree of deformation, so lower contact resistance is often accompanied with



▲ Fig. 3 Shows the Plan-View of switch with a doubly supported cantilever beam above a coplanar waveguide.

stronger adhesion. RF switches carry RF signals, so in certain operation conditions, such as impedance mismatch, a high level of RF power will pass through the switches. In such cases, the heat generated by RF power may cause micro-melting of asperities and could potentially short the contact points.

Before the integration of metal-to-metal switches into 5G mmWave communication systems become a reality, the adhesion (stiction) problem and reliability associated with the contacts needs to be resolved. The possible techniques for reducing the surface adhesion is either by selecting contact materials with less adhesion by applying chemical surface treatment or eliminating contamination with plasma cleaning.

Figure 1 illustrates a typical example of a cantilevered out-of-plane MEMS switch. Figure 1a is a cross-sectional view of the switch along X-axis; Figure 1b is a top view of the switch; and Figure 1c is a cross-sectional view of the switch along Y-axis. The typical MEMS switch is formed over a coplanar waveguide 101 in which a signal line 110 is formed between ground planes 102, 104 on a substrate 105 as shown in Figure 1. The signal line 110 includes an input port 112 and

an output port 114 formed on opposing ends of the substrate 105. The cantilever switch includes a post 120 or anchor affixed to the substrate 105 and includes an extension extending over the substrate in a direction perpendicular to the signal line 110. The extension of the cantilever includes a bottom layer 125 of dielectric material, such as silicate and a top layer of conductive material 130, such as gold. The cantilever further includes a contact bump or dimple 135 positioned underneath the bottom dielectric layer 120 and in alignment with the signal line ports 112, 114. Thus, when the cantilever is bent downward, the dimple 135 contacts the signal line 110, thereby connecting the input and output ports 112, 114.

In addition to this, the MEMS switch depicted in Figure 1 also includes an electrostatic actuator (not shown) for actuating the cantilever by applying or removing a DC bias voltage between the cantilever and the ground 102, 104 of the coplanar waveguide 101. The cantilever bends downward and upward, in a direction toward and away from the signal line, respectively, in response to the applied voltage from the actuator. Other RF MEMS switches may rely on a lateral movement in order

TechnicalFeature

to bring the moveable part of a cantilevered switch toward or away from a contact. Each moving part and contact may be metal (resistive switch), or one may be metal while the other is dielectric (capacitive switch).

NEW MEMS SWITCH USING CAPACITIVE CONTACTS (METAL-INSULATOR-METAL)

Figures 2 and 3 show the side view and top view of capacitive contacts shunt MEMS switch with a doubly supported cantilever beam 210 formed above a coplanar waveguide formed on a substrate 201. As shown in Figure 2, the first end 212 and second end 214 of the beam 210 are supported by respective ground planes 202 and 204 formed in the coplanar waveguide. The middle of the beam 210 is suspended over a signal line 220 formed in the coplanar waveguide. The beam 210 is connected to an actuator (not shown) configured to apply a DC bias voltage across the beam 210 and the ground planes 202, 204. The DC bias voltage causes the beam 210 to deflect downward. The signal line 220 includes a conductive layer 222 covered by a thin dielectric layer 224, such as silicon nitride.

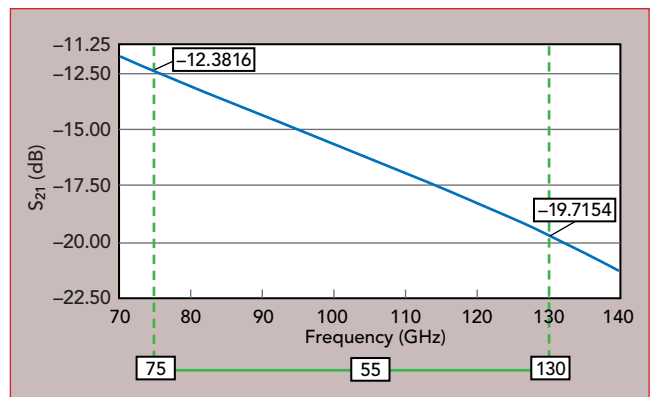
The dielectric layer is selected about $0.2\ \mu\text{m}$ thick. When the beam 210 deflects downward and contacts the signal line 220, a large shunt capacitance is obtained. The large shunt capacitance blocks RF signals from propagating along the signal line 220 of the coplanar waveguide (ON-state). When the DC bias is removed, the beam 220 deflects upward and returns to its original position, the shunt capacitance drops and the RF signal resumes propagating in unattenuated form (OFF-state).

In Figure 2, the beam 210 is made of molybdenum, and has a length of about $325\ \mu\text{m}$, a width of about $60\ \mu\text{m}$ and a thickness of about $1.2\ \mu\text{m}$. The signal line 220 extends through the coplanar waveguide and has a width (in the direction of the beam length) of about $60\ \mu\text{m}$. The beam 210 is suspended about $2.5\ \mu\text{m}$ above the signal line 220, thereby forming a $2.5\ \mu\text{m}$ air gap. The dielectric layer has a thickness of about $0.2\ \mu\text{m}$.

As shown in Figure 3, the beam 210 is perforated, having a grid of small perforations 301 in the middle and a large perforation 302, 303 at each end. The perforations yield improved downward deflection of the beam 210. It can be seen that vertical displacement of the beam 210 when the DC bias voltage is applied, which extends from no displacement at the respective ends 212, 214 of the beam, to about $0.91\ \mu\text{m}$ in the middle of the beam 210. The DC bias for the switch has been observed to be about 37 V.

Figure 4 shows the plot of the isolation characteristics of the switch in Figure 2 when the switch is open, across a band of mmWave signals from 75 to 130 GHz. The typical isolation is about $-12.4\ \text{dB}$ at 75 GHz, and about $-19.7\ \text{dB}$ at 130 GHz. The typical insertion loss of the switch when closed is about $0.74\ \text{dB}$ and return loss is about $10.04\ \text{dB}$. The actuation voltage needed for the switch can be further reduced by providing a different perforation arrangement.

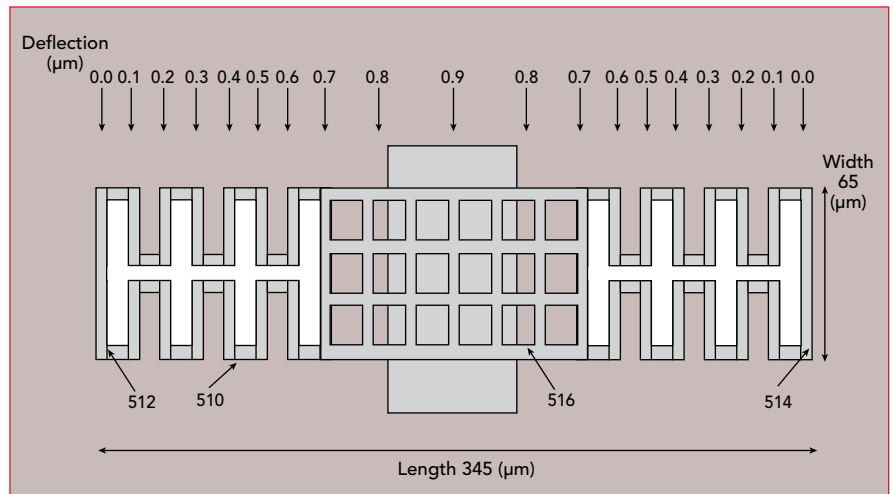
In the example of **Figure 5**, the MEMS switch includes a rectangular beam 510 made of gold and having a perforated structure. The middle portion 516 of the beam 510 forms a perforated grid or lattice. Each corner of the lattice structure then



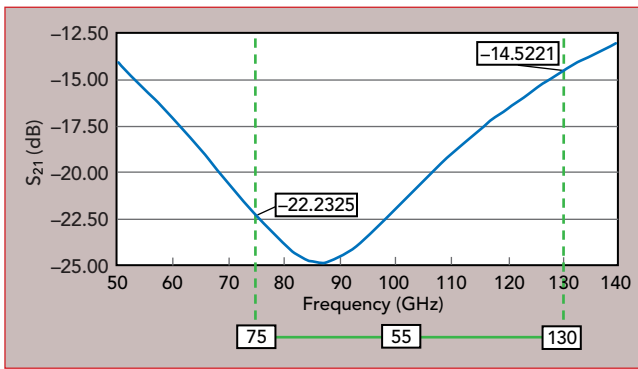
▲ Fig. 4 Shows the isolation plot of MEMS switch depicted in Figures 2 and 3.

extends in a serpentine pattern toward the first and second ends 512, 514 of the beam 510. The serpentine patterns on either end are then connected to one another, thereby forming first and second serpentine structures on either end of the beam 510. The serpentine structure permits for deflection of the beam with a lower bias voltage. The dimensions of the switch shown in Figure 5 are largely comparable to that of Figure 3 except that the beam of Figure 5 is slightly longer (about $345\ \mu\text{m}$), and slightly wider (about $65\ \mu\text{m}$). The beam still deflects downward up to $0.9\ \mu\text{m}$ but with only a 17 V bias voltage. The MEMS switch of Figure 5 exhibits improved isolation characteristics.

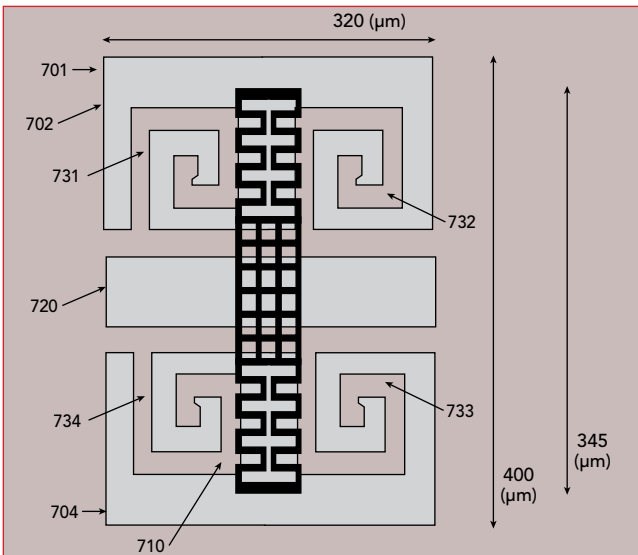
Figure 6 shows isolation characteristics of the switch of Figure 5 when the switch is open, across the 75 to 130 GHz band. Isolation is about $-22\ \text{dB}$ at 75 GHz, about $-14.7\ \text{dB}$ at 130 GHz and drops to as little as about $-24.8\ \text{dB}$ at 86 GHz. Inser-



▲ Fig. 5 Plan-View of capacitive shunt switch using a serpentine structure in the cantilever beam.



▲ Fig. 6 Shows the isolation plot of MEMS shunt switch in Figure 5.



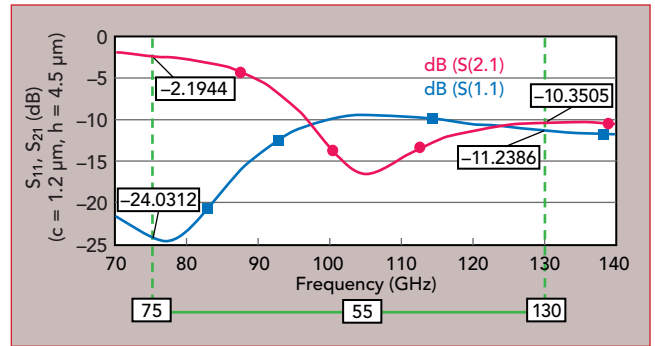
▲ Fig. 7 Shows the Plan-View of the DGS inspired MEMS switch.

tion loss of the switch when closed is only about 0.6 dB and return loss is about 15.15 dB.

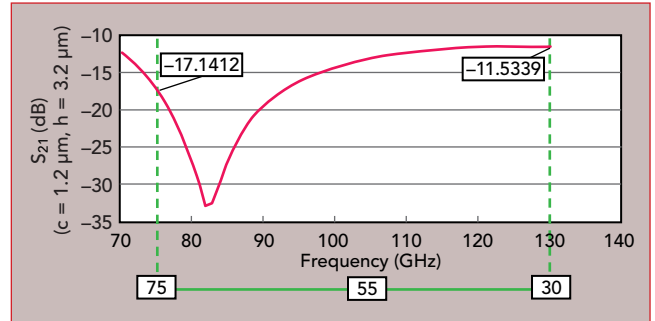
NEW DGS CAPACITIVE MEMS SWITCH

The isolation characteristics of these new shunt switches can be further improved by incorporating DGS, particularly in the mmWave frequency band of 75 to 130 GHz. A two-dimensional DGS is formed in each of the ground planes 702 and 704 of the MEMS switch shown in **Figure 7**. The DGS essentially behaves as a band stop filter, thereby affecting the transmission characteristics of the switch. Figure 7 includes a beam 710 having the same structural arrangement as the beam 510 of Figure 5 and formed on a ground plane structure 701 measuring about 320 μm long by about 400 μm wide. The ground plane structure 701 includes a signal line 720 between two ground planes 702, 704. In the example of Figure 7, the DGS forms four spiral shaped slots 731, 732, 733, 734 in a two-by-two grid and having mirror symmetry along the lengthwise axis of the signal line 720. Each of the spiral shaped slots have a common, uniform width.

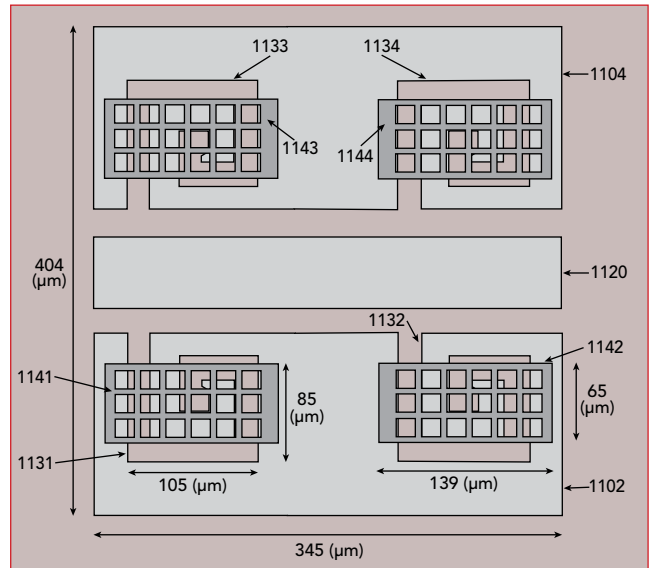
Figure 8 shows insertion loss and return loss of the switch in Figure 7 when the switch is closed. The typical insertion loss is 2.2 dB at 75 GHz and 10.4 dB at 130 GHz, but drops as low as 16.6 dB at 105 GHz. Return



▲ Fig. 8 Shows the return loss and insertion loss of MEMS switch in Figure 7.



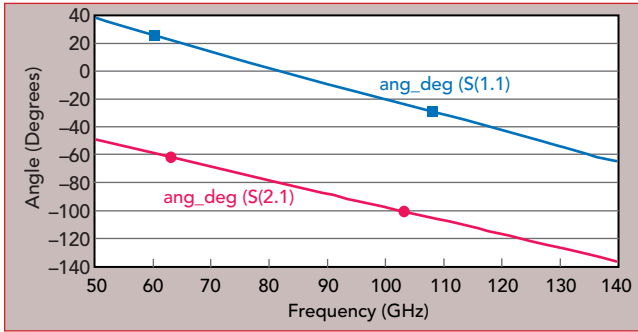
▲ Fig. 9 Shows the isolation of MEMS switch in Figure 7.



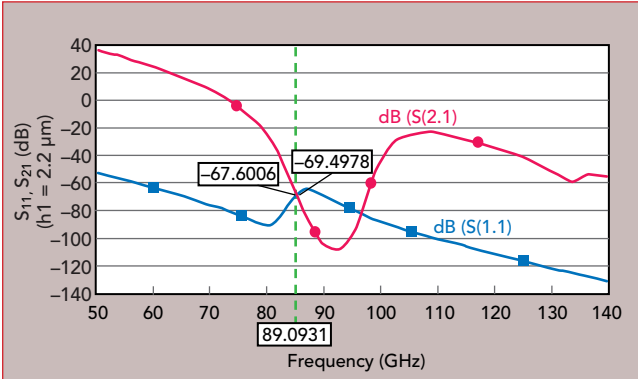
▲ Fig. 10 Shows the Plan-View of a switch, secondary MEMS switches are placed above the DGS.

loss is about 24 dB at 75 GHz and about 11.2 dB at 130 GHz but increases to about 9.5 dB at 105 GHz. **Figure 9** shows isolation for the DGS inspired MEMS switch illustrated in Figure 7 when the switch is open. Isolation is about -17.1 dB at 75 GHz and about -11.5 at 130 GHz and drops as far as about -32.5 dB at 82 GHz. Although isolation characteristics of the switch of Figure 7 show improvement, higher insertion loss limits the applications. To overcome the insertion loss, variation to the DGS structures are incorporated to **Figure 10**.

The MEMS switch shown in Figure 10 is similar in structure to that of Figure 7. As illustrated in Figure 10, the MEMS switch has two ground planes 1102, 1104



▲ Fig. 11 Transmission and reflection phase for the coplanar line of a switch without DGS.

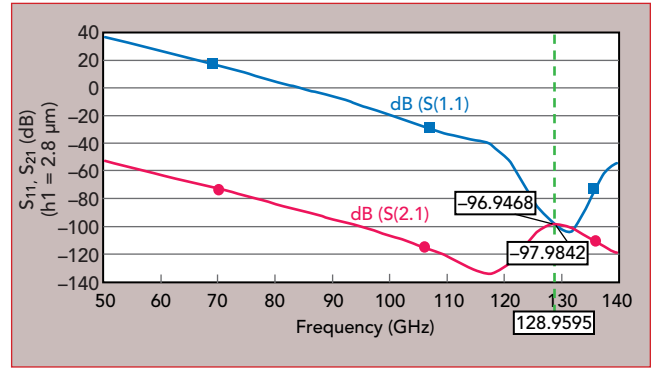


▲ Fig. 12 Plots of the transmission and reflection phase for the coplanar waveguide with DGS in Figure 10 for a height 2.2 μm .

bisected by a signal line 1120 and has four DGS structures 1131, 1132, 1133 and 1134 formed in the ground planes. The length of the ground planes and signal line are about $340 \mu\text{m}$, and the cumulative width of the switch is about $404 \mu\text{m}$. MEMS switch as shown in Figure 10 differs from Figure 7 in that each of the DGS structures includes a secondary MEMS switch 1141, 1142, 1143, 1144 positioned above the DGS structure. The shape of both the secondary switch and DGS may be rectangular, but the secondary switch may be longer while the DGS structure may be wider. In the example of Figure 10, each DGS structure is a perforated lattice, and is about $105 \mu\text{m}$ in length and about $85 \mu\text{m}$ in width, overlaid by a secondary switch that is about $139 \mu\text{m}$ in length and $65 \mu\text{m}$ in width. The MEMS switch described in Figure 10 includes a substrate 1101 on which the ground plane is formed. The ground plane has a thickness or height of about $2 \mu\text{m}$.

Although not shown, the slots of the DGS structure 1131 are formed in the ground plane and may have a depth equal to the height of the ground plane 1102. A secondary switch 1141 is formed above the DGS structure 1131. As depicted in Figure 10, the secondary switch 1141 includes a beam 1151 supported by two feet 1162, 1164. The supporting feet have a height of about $1 \mu\text{m}$, thereby raising the beam 1151 about $1 \mu\text{m}$ above the DGS and ground plane. Thus, there is an air gap of about $1 \mu\text{m}$ between the non-deflected beam and the DGS positioned below. The beam thickness or height of the beam 1151 may be about $1.2 \mu\text{m}$.

The beam 1151 shown in Figure 10 is connected to an actuator (not shown) to supply a bias voltage, which



▲ Fig. 13 Plots of the transmission and reflection phase for the coplanar waveguide with DGS in Figure 10 for a height $2.8 \mu\text{m}$.

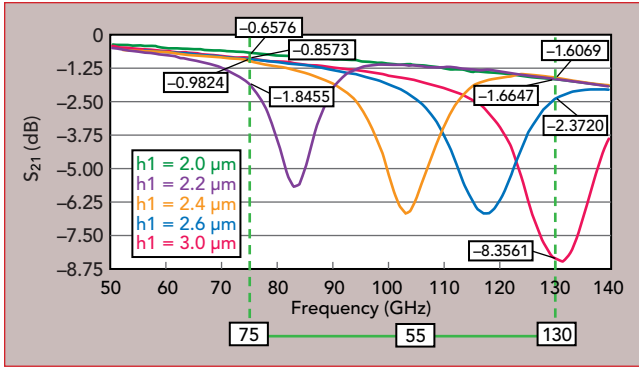
runs from the beam 1151 to the ground plane 1102 via the feet 1162, 1164. Applying the bias voltage causes the beam 1151 to deflect downward toward the ground plane 1102, thereby affecting the capacitive characteristics of the DGS structure 1131. The amount of voltage applied to the switch 1101 may be continuously variable and thus the capacitive characteristics of the DGS structure (and its effect on the main MEMS switch of the device) can be varied or tuned.

It has been found that the switch arrangement of Figure 10 behaves like a metamaterial (engineered material). This can be seen by first analyzing the transmission and reflection phases of a signal line formed in a coplanar waveguide without the DGS structure of Figure 10, and then analyzing the transmission and reflection phases of the same signal line with the DGS structure of Figure 10.

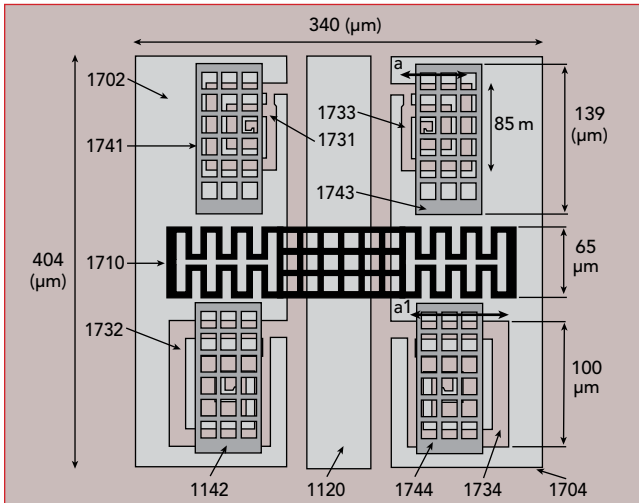
For a simple coplanar line without DGS, the transmission and reflection phase are analyzed. The results are shown in **Figure 11**; the transmission and reflection phases of a signal transmitted across a coplanar waveguide without the DGS structure over a band of mmWave frequencies from 50 to 140 GHz. As shown, any shift in the transmission phase of the signal is met with a substantially equal (within about 20 degrees) shift in the reflection phase.

Figure 12 shows transmission and reflection phases of a signal over the same band of frequencies for the same coplanar waveguide but with the DGS structure incorporated into the waveguide at a height of $2.2 \mu\text{m}$, which is the distance from the top surface of the substrate (the basin of the slots of the DGS structure) to the bottom surface of the secondary switch positioned above the DGS structure. The transmission and reflection phases do not shift equally across the band of frequencies, and even shift in opposite directions, eventually crossing one another at 85 GHz and then crossing back at 96 GHz.

Figure 13 shows transmission and reflection phases for the same coplanar waveguide but with the DGS structure at a height of $2.8 \mu\text{m}$. The transmission and reflection phases shift substantially equally until about 110 GHz, but then begin shifting in opposite directions at frequencies above 115 GHz and even cross one another at about 128 GHz. The resonance frequency of the DGS structure thus varies depending on the height



▲ Fig. 14 Plots of isolation characteristics for five secondary switches positioned over DGS structures at varying heights.



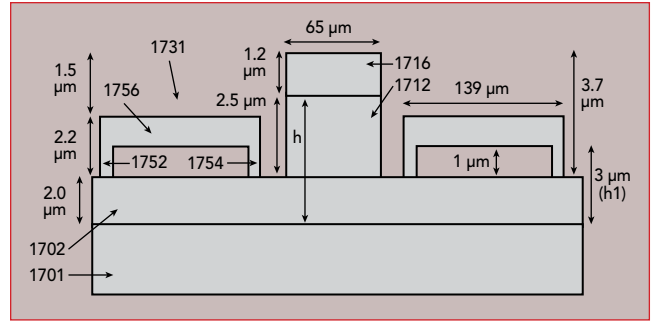
▲ Fig. 15 A top view of a metamaterial inspired switch having a DGS and secondary switches in accordance with an aspect of the new structure.

of the air gap between the ground plane and the beam.

Figure 14 shows a plot of isolation characteristics for five secondary switches positioned over DGS structures at varying heights. The resonant frequency of the structure is shown to shift to higher frequencies as the air gap between the ground plane and beam increases.

An example MEMS shunt switch with DGS structures and overlaid secondary switches is shown in complete form in Figure 15, which includes a signal line 1720 positioned between a first ground plane 1702 and a second ground plane 1704, the signal line separated from each ground plane by first and second spaces 1703, 1705, respectively. A primary shunt switch 1710 is positioned on top of, is connected to and bridges the first and second ground planes 1702, 1704. The primary shunt switch 1710 runs perpendicular to, and is suspended over, the signal line 1720. When a bias voltage is applied to the primary shunt switch 1710, the switch 1710 deflects downward toward the signal line 1720. When the bias voltage is not applied, the switch 1710 deflects back upward to its original position.

A first DGS structure 1731 and a second DGS structure 1732 are formed in the first ground plane 1702. A third DGS structure 1733 and a fourth DGS structure 1734 are formed in the second ground plane 1704. The first and third DGS structures 1731, 1733 have mirror symmetry along a lengthwise x-axis of the primary



▲ Fig. 16 Side view of the switch shown in Figure 15.

switch 1710 and are a similar shape. The second and fourth DGS structures 1732, 1734 also have mirror symmetry along a lengthwise x-axis of the primary switch 1710 and are a similar shape.

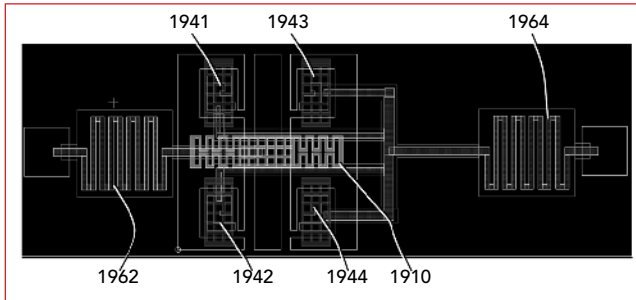
In the example of Figure 15, the first and third DGS structures 1731, 1733 are a different size from the second and fourth DGS structures 1732, 1734. The second slots of the first and third DGS structures 1731, 1733 are about 85 μm long, whereas the second slots of the second and fourth DGS structures 1732, 1734 are about 100 μm long. The third slots of the first and third DGS structures 1731, 1733 are also shorter than those of the second and fourth DGS structures 1732, 1734. This contrasts with the four DGS structures shown in each of Figures 7 and 10, which all have the same dimensions.

Each DGS structure is overlaid by a respective secondary shunt switch 1741, 1742, 1743, 1744. Each secondary shunt switch is connected to its respective ground line and is suspended over its respective DGS structure with an air gap in between. The secondary shunt switches are rectangular, each of the secondary switches positioned lengthwise parallel to the signal line 1720 and perpendicular to the primary shunt switch 1710. The secondary switches positioned above the first DGS structure 1731 and the third DGS structure 1733 have a mirror symmetry with the secondary switches positioned above the second DGS structure 1732 and the fourth DGS structure 1734 along a lengthwise x-axis of the primary switch 1710. Additionally, the secondary switches positioned above the first DGS structure 1731 and the second DGS structure 1732 have a mirror symmetry with the secondary switches positioned above the third DGS structure 1733 and the fourth DGS structure 1734 along a lengthwise y-axis of the signal line 1720. The secondary shunt switches 1741, 1742, 1743, 1744 are also perforated. In the example of Figure 15, the switches have a grid-like lattice perforation.

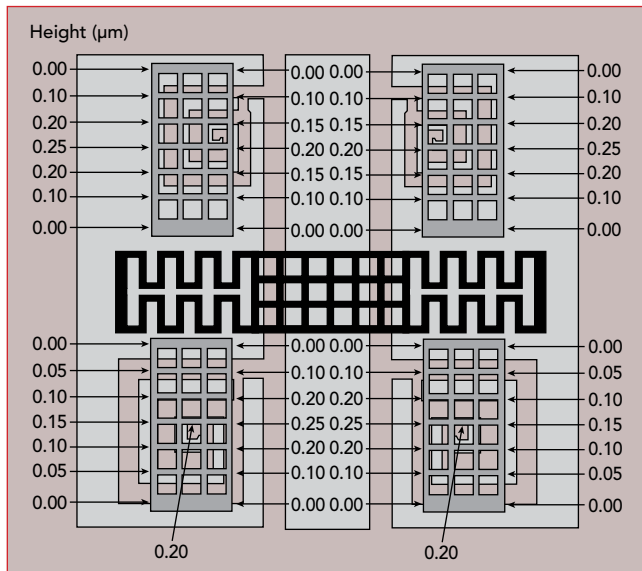
Figure 16 shows a side-view of the switch of Figure 15. The switch in Figure 15 is formed on a substrate 1701. A ground plane 1702 is formed over the substrate 1701, and the primary switch 1710 is formed on top of the ground plane 1702. The primary switch 1710 has two feet 1712 (the second foot is obstructed by foot 1712 in Figure 17) supporting a beam 1716. Two secondary switches 1731, 1732 are positioned on either side of the primary switch 1710. Each of the secondary switches also includes two feet 1752, 1754 supporting a beam 1756. DGS structures (not shown) are formed in the ground plane 1702 at respective positions underneath the secondary switches 1731, 1732.

Technical Feature

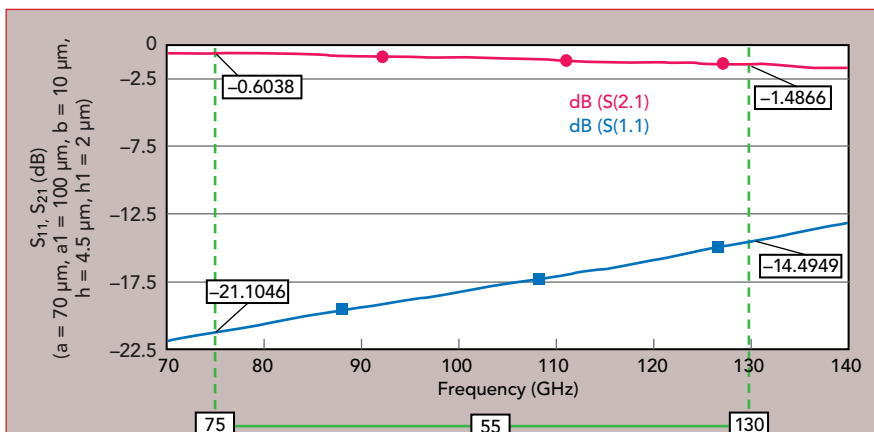
In the example of Figures 15 and 16, the substrate and ground planes have a length of about 404 μm , and a width of about 340 μm . The ground planes have a thickness of about 2 μm . The primary switch 1710 extends the length of the substrate, the primary switch feet 1712 and beam 1716 have a width of about 65 μm . The feet 1712 have a height of about 2.5 μm , and the beam 1716 has a thickness of about 1.2 μm . The secondary switches 1731 have a length of about 139 μm , and the secondary switch feet 1752, 1754 and beam 1756 have a width of about 65 μm . The feet 1752 have



▲ Fig. 17 Example layout of the metamaterial inspired MEMS switch.¹



▲ Fig. 18 The amount of downward deflection at several points of the secondary switches (measured in μm) when the secondary switches are actuated.¹



▲ Fig. 19 Plot of return loss and insertion loss of the switch described in Figure 17 with the secondary switches activated.

a height of about 1 μm , and the beam 1756 has a thickness of about 1.2 μm . Thus, the entire switch in Figure 15 can be formed on top of the substrate 1701 within a 5.7 μm space.

NEW METAMATERIAL MEMS SWITCH

Figure 17 shows an example layout of a metamaterial inspired MEMS switch, showing the connections between the primary switch 1910 and secondary switches 1941-1944, a first actuator 1962 and a second actuator 1964. The first actuator 1962 is connected to the primary switch 1910 and configured to provide a bias voltage to the primary switch. The second actuator 1964 is connected to each of the secondary switches 1941-1944 and is configured to provide a bias voltage to the secondary switches.

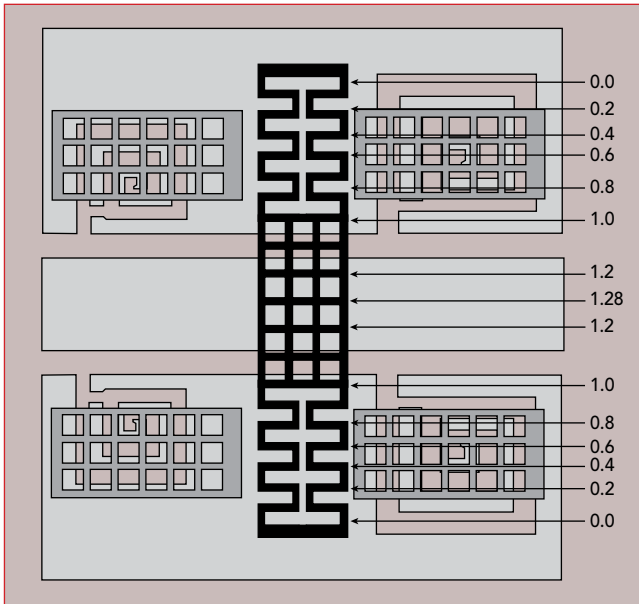
In operation, the primary switch shown in Figure 17 may be either ON (bias voltage provided from the first actuator 1962) or OFF (no bias voltage provided by the first actuator 1964). When the primary switch is ON, the primary switch beam deflects downward, resulting in a large shunt capacitance that blocks RF signals from propagating along the signal line 1920. When the primary switch is OFF, the primary switch beam deflects back upward (at rest), reducing the shunt capacitance and permitting RF signals to propagate along the signal line 1920.

When the primary switch 1910 is OFF, the secondary switches 1941-1944 may be turned ON in order to negate the effects of the DGS structures toward insertion and return loss. A bias voltage is applied from the second actuator 1964 to each of the secondary switches 1941-1944, thereby causing the switches to deflect downward toward the DGS structures and create a shunt capacitance blocking the effects of the DGS structure.

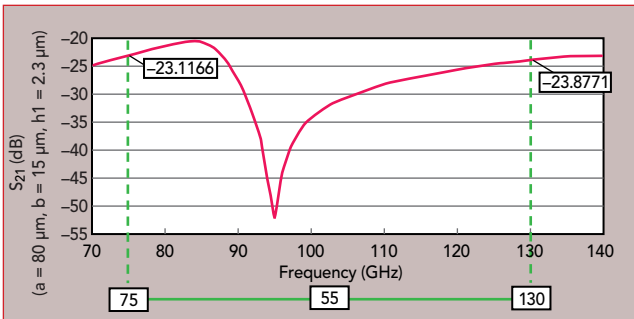
Figure 18 shows the amount of downward deflection at several points of the secondary switches (measured in μm) when the secondary switches are actuated. Figure 19 shows return loss and insertion loss characteristics for the MEMS switch illustrated in Figure 17 when the primary switch is OFF, and the secondary switches are ON. At 75 GHz, insertion loss is as low as about 0.6 dB and return loss is as low as about 21.1 dB. At 130 GHz, insertion loss is still relatively low at about 1.5 dB, and return loss is also relatively low at 14.5 dB. Returning to Figure 17,

when the primary switch 1910 is ON, the secondary switches 1941-1944 may be turned OFF in order to get the benefit of the DGS structures toward isolation. No bias voltage is applied from the second actuator to the secondary switches 1941-1944, so the switches remain separated from the DGS structures underneath by the airgap.

Figure 20 shows the amount of downward deflection at several cross-sections of the primary switches (measured in μm) when the primary switch is actuated. Deflection along the entire width of the primary switch is uniform for any given point along the length of



▲ Fig. 20 The amount of downward deflection at several cross-sections of the primary switches (measured in μm).

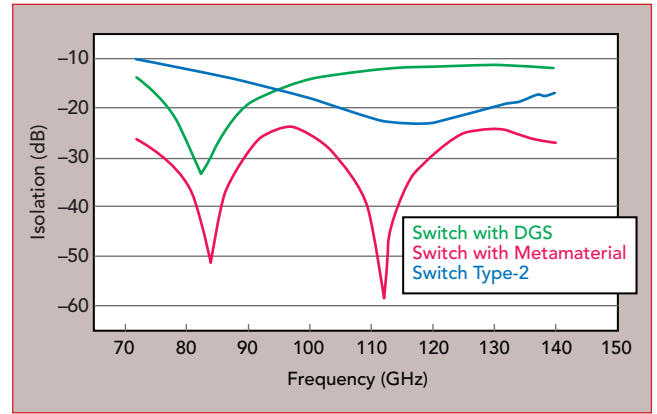


▲ Fig. 21 The isolation characteristics of the switch of Figure 17 having varying air gap heights.

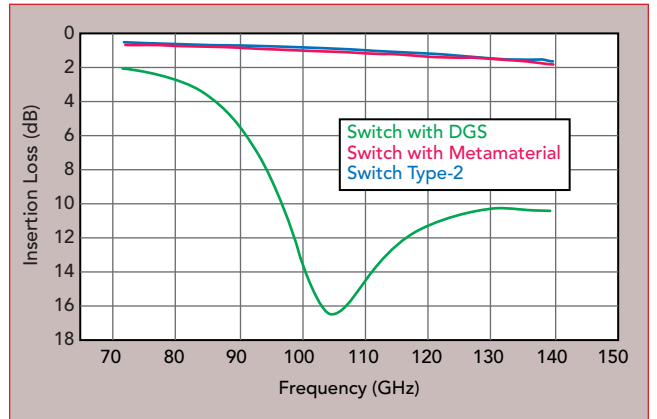
the switch.

Figures 21 and 22 show the isolation characteristics for the MEMS switch in Figure 17 when the primary switch is ON and the secondary switches are OFF. In Figure 21, the same DGS structure is used. This leads to a significant improvement in isolation at a relatively narrow band (e.g., less than about 10 GHz, between 90 and 100 GHz). At 75 GHz isolation is about -23.1 dB and at 130 GHz, isolation is about -23.9 dB. But at about 95 GHz, isolation is improved to about -52 dB.

Figures 22 and 23 show plots of isolation and insertion loss characteristics for MEMS switch utilizing different structures. The metamaterial construction leads to an overall improvement of isolation over a wider band of frequencies. The structure represented in Figure 15 yields improved isolation at about 84 GHz (about -51 dB) and at about 112 GHz (about -59 dB) and is not worse than about -24 dB between 75 and 130 GHz. The insertion loss characteristics of the DGS switch is poor compared to the regular switch and metamaterial versions.



▲ Fig. 22 Isolation characteristics for switches with different topologies.

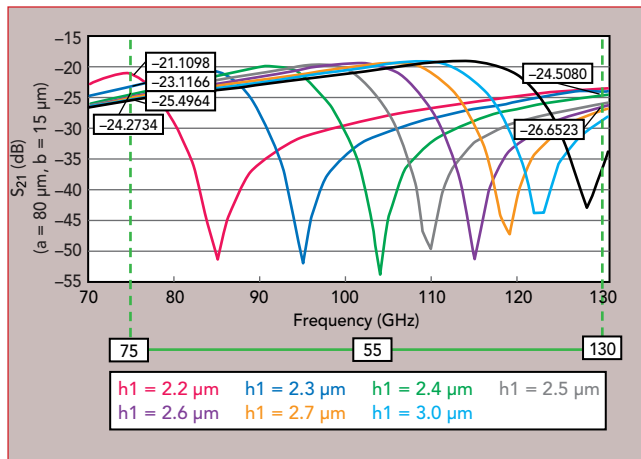


▲ Fig. 23 Insertion loss characteristics for switches with different topologies.

Switch Type 2 is the first version of the new MEMS Switch using Capacitive Contacts.

As seen from the attenuation characteristics of Figures 19 and 21, providing DGS structures with capacitive MEMS shunt switches above the DGS structures is an effective way of incorporating the benefits of DGS for improved isolation when RF signals are blocked, while at the same time negating the detriments caused by the DGS to insertion loss and return loss when RF signals are propagating. In this respect, incorporation of DGS structures and corresponding shunt switches are an improvement to RF MEMS design and operation.

TABLE 1 COMPARISON OF MEMS SWITCHES PERFORMANCE				
Parameters	Shunt Switch (Figs. 2-3)	Shunt Switch (Fig. 5)	Shunt Switch + DGS w/o Switches (Fig. 7)	Shunt Switch + DGS w/ Switches (Fig. 17)
Actuation Voltage	37 V	17 V	17 V	17 V
Isolation (75-130 GHz)	-12 to -19 dB	-15 to -24 dB	-11 to -32 dB	-24 to -59 dB
Insertion Loss	0.74 dB	0.6 dB	-2 to -11 dB	0.6 dB
Material	Molybdenum	Gold	Gold	Gold
Cantilever Height	2.5 μm	2.5 μm	2.5 μm	2.5 μm



▲ Fig. 24 Isolation characteristics for various MEMS switch designs.

Table 1 provides a summary of the actuation voltage, isolation and insertion loss characteristics for the above-described switch designs with air gaps (and cantilever beam heights) of about $2.5 \mu\text{m}$.¹

Figure 24 shows isolation characteristics for several switches having different DGS and secondary switch arrangements, in which both switches are actuated. Actuating the secondary switch results in improved isolation characteristics over a narrow band of frequencies. The band at which the improved isolation occurs varies depending on the air gap height between the switches and DGS structures. As the air gap increases, the frequency band at which the best isolation for the switch occurs shifts upward. For an air gap of $2.2 \mu\text{m}$, isolation of about -52 dB

is achieved at about 85 GHz and for an air gap of $3.0 \mu\text{m}$ isolation of about -44 dB is achieved at about 122 GHz . This demonstrates the relative flexibility of the proposed combination of DGS structures with secondary switches for providing improved isolation across a wide range of high frequencies.

CONCLUSION

In Part I of this three-part series, it is shown that both the DGS structures and secondary switches can achieve improvements in insertion loss and isolation. These improvements contrast with the tradeoffs conventionally seen when using either only a shunt switch (good insertion loss, poor isolation) or only a DGS structure (improved isolation, but worse insertion loss). The proposed combination of a primary shunt switch, DGS structures and secondary shunt switches is shown to behave like a metamaterial. In addition to this solution, it also improves resistance to stiction of the MEMS switch using metamaterial layers within the design of the switch contacts which will be covered in detail in Parts II and III. ■

References

1. Shiban Koul, Ajay Poddar and Ulrich Rohde, "Microelectromechanical Switch with Metamaterial Contacts," *US Patent Pub. No. 02161415A1*.
2. Astrid Lambrecht, "The Casimir Effect: a Force from Nothing," *Physics World*, September 2002.
3. F. Intravaia and C. Henkel, *New Frontiers of Casimir Force Conference*, Santa Fe, New Mexico, 2009.
4. U. Leonhardt and T. G. Philbin, "Quantum Levitation by Left-Handed Metamaterials," *New J. of Physics*, August 2007.
5. Mercado et. al., "A Mechanical Approach to Overcome RF MEMS Switch Stiction Problem," *ECTC 2003*.
6. Chaitanya Mahajan, "Design and Analysis of RF MEMS Switches (70 GHz to 130 GHz), M.Tech dissertation, CARE, IIT Delhi, May 2018.